Front. Optoelectron. 2015, 8(1): 81–92
DOI 10.1007/s12200-014-0446-y

RESEARCH ARTICLE

Terahertz pulse imaging in archaeology

J. Bianca JACKSON (✉)[1,2], Julien LABAUNE[1], Rozenn BAILLEUL-LESUER[3], Laura D'ALESSANDRO[3], Alison WHYTE[3], John W. BOWEN[2], Michel MENU[4], Gerard MOUROU[1]

1 Institute de la Lumière Extrême, Ecole Polytechnique, Palaiseau, France
2 School of Systems Engineering, University of Reading, Reading, UK
3 Oriental Institute, University of Chicago, Chicago, IL, USA
4 Centre de Recherche et de Restauration des Musées de France, Paris, France

Abstract The work presented in this paper was performed at the Oriental Institute at the University of Chicago, on objects from their permanent collection: an ancient Egyptian bird mummy and three ancient Sumerian corroded copper-alloy objects. We used a portable, fiber-coupled terahertz (THz) time-domain spectroscopic imaging system, which allowed us to measure specimens in both transmission and reflection geometry, and present time- and frequency-based image modes. The results confirm earlier evidence that THz imaging can provide complementary information to that obtainable from X-ray computed tomography (XRCT) scans of mummies, giving better visualisation of low density regions. In addition, we demonstrated that THz imaging can distinguish mineralized layers in metal artifacts.

Keywords terahertz (THz), time-domain imaging, spectroscopy, non-destructive evaluation, archaeology

1 Introduction

Terahertz pulse imaging and spectroscopy (TPIS) is emerging as a nondestructive-evaluation tool of high growth potential within the fields of art conservation, historical architecture conservation, and archeology [1]. In particular with mummies, TPIS has been explored as an alternative — or complement — to X-ray imaging techniques [2,3]. It is the combination of material characterization, time of flight imaging, and the penetration of optically opaque materials that gives rise to applications for subsurface imaging of many culturally significant objects. Moreover, the variety and adaptability of the many electronic, optical, and hybrid terahertz (THz) sources allow for versatile approaches to measurement [4–6]. Spatial resolution for free-space THz measurements can be scaled from tens of micrometers to several millimeters, providing the possibility of taking measurements without sample extraction, in situ, and in the field [7]. Lastly, moderate exposure to THz radiation poses significantly less long-term risk [8,9] to the molecular stability of the historical artifact and to humans than X-rays, ultra violet (UV) or visible radiation, because it is non-ionizing and produces low thermal heating. Therefore, THz technology provides a non-ionizing, noninvasive, noncontact, non-destructive toolset [10] for the examination of unique and priceless objects [11].

The THz region is possibly the least understood and most complicated part of the electromagnetic spectrum. The THz region has been typically defined as being between 30 μm and 3 mm in wavelength, thus putting its scale on the border between the microscopic and macroscopic world. At frequencies between 0.1 and 10 trillion (10^{12}) cycles per second, the THz regime overlaps with both the microwave and far infrared regions of the spectrum. The THz regime also corresponds to photon energies between 0.4 and 40 meV. Lower frequency microwave radiation has lower photon energy, therefore the photons cannot be measured directly, only collectively by the electrical bias they induce in a detector. On the other hand, infrared radiation is optical, since its photon energy is large enough that individual photons can be directly measured. Thus, THz radiation uniquely straddles the worlds of electronics and optics. Over the last two decades, means of producing and detecting sub-picosecond, broadband pulses of THz radiation by integrating optoelectronic devices with ultrafast optical lasers have sparked many new forms of research — including time-domain THz spectroscopy and imaging. As the THz technology gap is filled by diverse and practical devices, the number of THz

Received May 26, 2014; accepted July 18, 2014

E-mail: jbiancajackson@gmail.com

applications constantly increases, including those developed for the chemical-mapping of pharmaceuticals, the non-destructive evaluation of space shuttle foam, people-safe security imaging, and atmospheric-chemical species monitoring [12,13].

Our TPIS technique is based on time-domain spectroscopy (TDS). The THz pulse is measured as a transient electric field, which can be directly transformed into the amplitude and phase spectra of the pulse. When the THz pulse is transmitted through an object of low electrical conductivity (thus relatively low absorption), compositional changes — which include refractive index and optical density — can result in changes of the amplitude, shape and propagation time of the THz pulse. By scanning the object, this can be exploited to image the lateral and axial spatial features buried beneath the visibly opaque surface of the object. While the wide bandwidth of the THz pulses can aid in spectroscopically discriminating between buried materials that exhibit different THz-refractive-index spectra, the short-time-duration nature of THz pulses can also help isolate and distinguish depth information from different interfaces within an object.

In the course of our study, we were permitted access to the conservation laboratory of the Oriental Institute at the University of Chicago to examine several archeological artifacts from their collection. The first is an Egyptian neonate bird mummy (OIM E9164, Fig. 1), which was to be included in a project to image several dozen bird mummies using X-ray computed tomography (XRCT) [14]. Challenges of such an endeavor included protecting the fragile objects from physical disturbance and fluctuations in humidity. Special packaging and precise coordination of transport to the medical imaging facilities were essential to the XRCT experiments. In contrast, the availability of portable THz-TDS systems enabled our measurements to be performed in the well-controlled environment of the conservation laboratory.

Fig. 1 Photograph of ancient Egyptian bird mummy (OIM E9164) [15]

Among the other selections, we studied corroded copper-alloy (most likely bronze) artifacts from Ancient Sumer (now Iraq), with special attention toward a 5 cm fragment from an unregistered object (Fig. 2) and two cups (Fig. 3). For many archeological artifacts made of bronze or other copper-based alloys, the corrosion process can produce multilayer oxide structures (Fig. 4) — such as copper + cuprite + copper trihydroxy chloride minerals + malachite + azurite — which through time and environmental exposure can entirely convert the metallic material to stratified, composite layers of dielectric minerals [16,17]. This particular application for TPIS is dependent on the ability of THz waves to distinguish dielectric corrosion products from their metallic source material by their transmissivity and reflectivity. Previous work has been done to find defects beneath the coating on metal surfaces [18,19], however not much THz research has been conducted to study the specific corrosion layers themselves. THz pulses have the potential to spectroscopically identify and spatially distinguish each layer.

2 Experimental methods

Our time-domain THz imaging system consists of computer-controlled, motorized translation stages and the Picometrix T-Ray 4000 (TR4K) commercial THz time-domain spectrometer. The modelocked, two-stage, amplified, Ytterbium fiber laser operates with a center frequency near 1064 nm, a 100 fs pulse width, a 50 MHz repetition rate and a maximum output power of 400 mW.

The THz pulses were generated and then propagated through free-space using a biased, photoconductive switch antenna, consisting of a photosensitive low-temperature grown gallium arsenide semiconductor with two metal electrodes deposited on its surface. The antenna is illuminated at normal incidence by the ultrafast laser pulse, thus generating electron-hole pairs into the semiconductor. A voltage bias is applied to the electrodes to generate a photocurrent. The free-space THz electromagnetic field emanating from the antennas is proportional to the rapid change in the photocurrent — the sub-mechanisms of which determine the THz pulse's duration and bandwidth. A second photoconductive antenna is used as the THz receiver. The optical pulse generates photocarriers in the receiver by the same photoexcitation mechanism as when the emitter is illuminated. However in this case, the incident electric field of the THz pulse causes a time-varying potential to develop across the receiver, thus serving as an applied voltage bias that induces a transient photocurrent, which is amplified and measured as an electrical signal by using a data acquisition board and computer.

The development of compact, fiber-coupled THz-TDS systems, such as the TR4K, has several benefits which were essential to the advancement of THz applications in art and archeology. As a general rule, cultural heritage conservators aim toward minimizing the disturbance of the objects under investigation. The optical components for the compact spectrometer are contained within an easy to transport (size and weight) box. This allows for lower

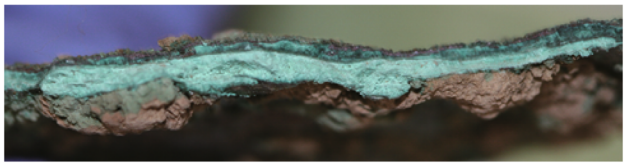

Fig. 2 Photo of corroded copper-alloy fragment cross-section [17]

(a) (b)

Fig. 3 Photographs of corroded copper-alloy (a) cup A (OIM A11280A, 12 cm diameter) and cup B (OIM A11399A, 10 cm diameter) [17]

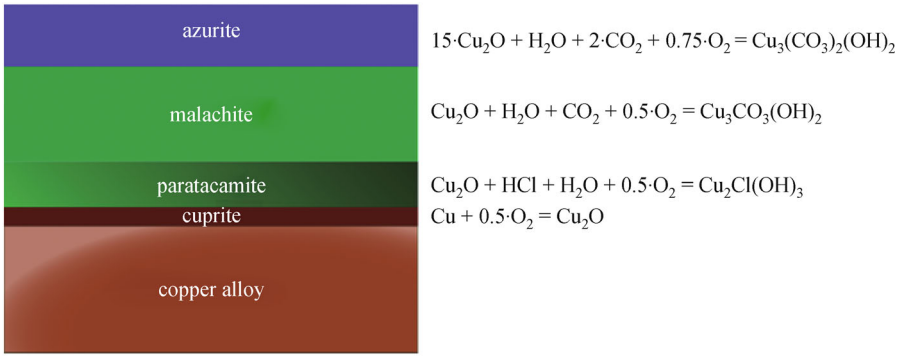

Fig. 4 Diagram of typical copper-based corrosion layers

complication on-site or field measurements. The fiber-coupled THz antennas permit rapid modification of the measurement geometry from transmission (Fig. 5(a)) to reflection (Fig. 5(b)), and vice versa. Additionally, it makes it possible for the object to remain fixed and secure during the scans, and facilitates the measurement of large objects in the transmission geometry.

We took into consideration the relatively low THz absorption and refractive indices of polystyrene foam [20] and paper [21] and utilized a foamcore support (Fig. 5(a)), which could permit us to securely scan the top and bottom of the extremely fragile mummy in transmission with minimal consequence to the signal. Figure 6(a) shows THz time-domain signals through the ambient environment and the foam support. The THz spectra (Fig. 6(b)) are obtained by performing a fast Fourier transform of the time domain signals. The refractive index and absorption of the foamcore (Fig. 6(c)) were ~20% and ~1500% higher than expected, respectively. This may be due to the thickness, type and coating of the board's paper shell. For future experiments, a several millimeter thick sheet of uncoated, un-sheathed polystyrene, or polymethyacrylimide [22], would provide equally rigid support with less signal loss.

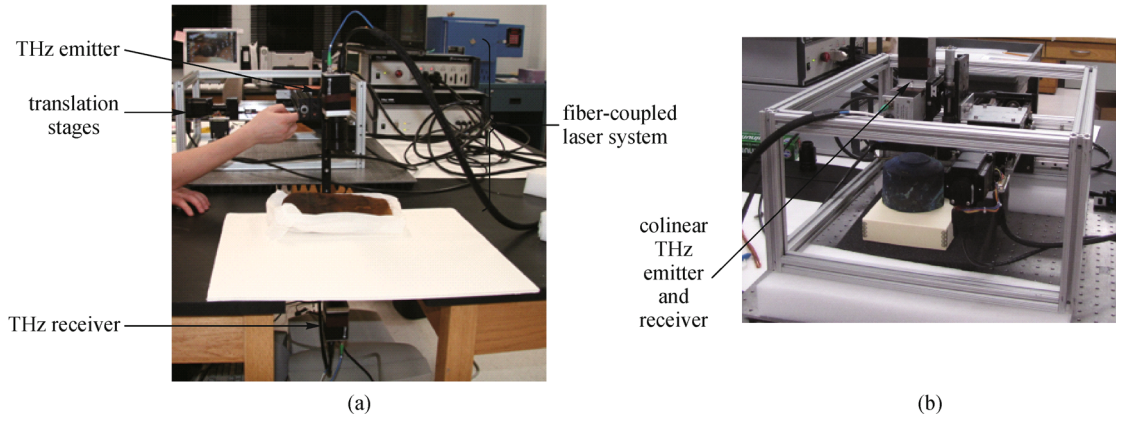

Fig. 5 Photographs of the (a) transmission [15] and (b) reflection setups

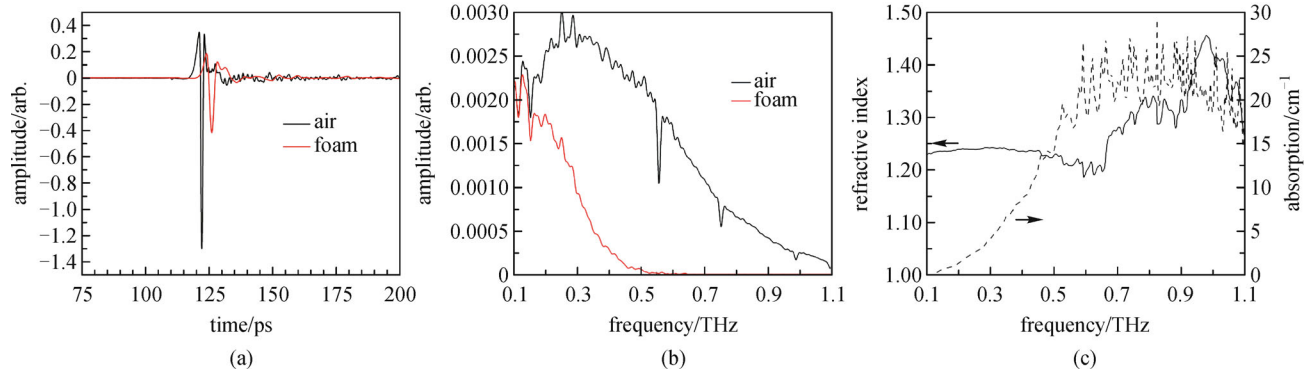

Fig. 6 Air and foam support reference (a) time domain signal; (b) transmission spectra and (c) refractive index and absorption spectra for the foam support

3 Discussion

3.1 Terahertz pulse imaging of a bird mummy

Transmission through the thicker, upper region of the mummy was too small to discern a signal through the baseline noise, so we only scanned the lower 80%. The two dimensional scans of the middle and lower regions can be seen in Fig. 7, and were calculated using the amplitude of the minimum peak for each pixel. The spatial resolution, or ability to see detail in the image, was negatively impacted by decreased bandwidth of the signal, as well as the changing spot size of the Gaussian beam through the bird. For the torso region, there is very strong absorption loss where the skeleton and desiccated organ tissue would be (black). For the leg region, the flesh and bone are less dense, resulting in better signal to noise and more distinct features. The shape of what appear to be the claws (although probably tibio-tarsal joints), however, is the most impressive feature of this image.

Figure 8 shows exemplary signals through the middle region, or torso, and lower region, or legs, of the bird mummy, designated by the letters A – H in Fig. 7. The multiple peaks, seen in Figs. 8(a) and 8(b), are a result of internal reflections of the THz pulse as it interacts with the textile wrap, desiccated flesh and bones of the bird. Note the one order of magnitude difference in transmission between the torso region and the leg region. The spectra in Fig. 8(c) also show significant signal loss above 0.2 THz, even in the "empty" region H, which suggests the loss is most likely due to the electric field being scattered by the weave and layers of the cloth wrapping [23]. Fortunately, in the range of 0.1 to 0.2 THz, the attenuation of the foam support is comparable to air.

There are few published comparisons of mummies imaged using both X-rays and THz radiation. Previously, Öhrström et al. also used THz transmission imaging to view the contents of a mummified human hand and fish [2]. They demonstrated that with TPIS it was possible to recognize differences in the desiccated flesh and that it adds a temporal aspect that does not exist in other techniques, despite TPIS having coarser resolution than XRCT. Fukunaga et al. also confirmed that THz imaging may complement X-ray images when materials with low radiographic density and contrast are being investigated [3]. From the XRCT images taken on this bird mummy (Fig. 9), we can confirm this with significance. It is likely that since the bird was young at the time of its death, its

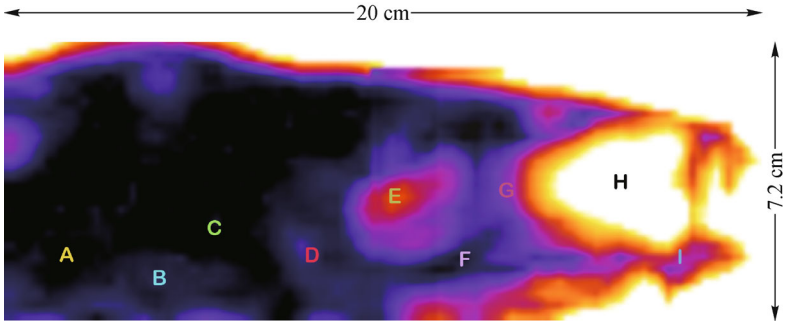

Fig. 7 Terahertz transmission image of bird mummy {color scale: white/yellow = higher transmission, black/violet = lower transmission}

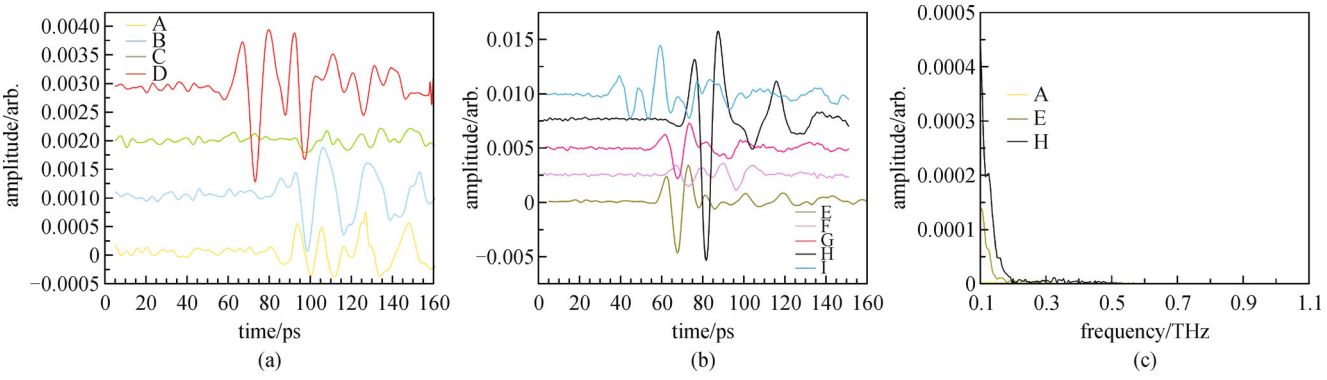

Fig. 8 Select (offset) time-domain waveforms from (a) torso region and (b) leg region; (c) spectral waveforms from bird mummy transmission signals

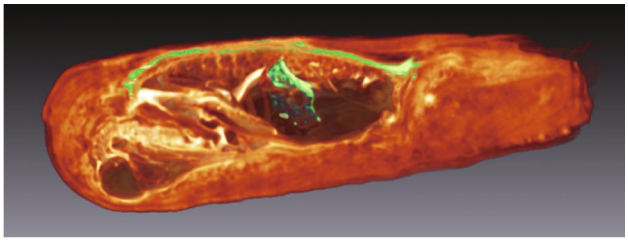

Fig. 9 X-ray computed tomography scan of Egyptian bird mummy E9164 [14] {Courtesy of Charles Pelizzari and Christian Wietholt}

bones were soft, resulting in low-density calcification. As a result, THz provides a much better visualization of the leg region of the bird than X-rays, as applied in this particular CT-scanning session [14]. Further comparative measurements using other X-ray energies and more intense THz waves would be desirable.

3.2 Corroded copper-alloy fragment

A copper alloy fragment from an Early Dynastic (~2000 BC) Sumerian unregistered object excavated from the Tell Agrab settlement of the Diyala Valley in Iraq (Fig. 2) was examined to determine whether it is possible to distinguish the metallic and mineralized stratified corrosion layers. Figure 10(a) shows an image of the surface of the fragment, calculated using the peak to peak amplitude of each pixel. The brightest areas are where the surface of the fragment is still metallic, due to the high reflectivity. The pink line indicates the location of the slice, seen as the cross-sectional b-scan in Fig. 10(b). Figure 10(c) shows the time-domain signatures of select point measurements. The outer crust is composed of calcified dirt, possibly tin and copper corrosion products. It is possible, however, to observe some significant reflectivity from the near-surface interfaces.

3.3 Corroded copper-alloy cups

Two Sumerian copper alloy cups excavated from the ancient city of Eshnunna — modern-day Tell Asmar in the

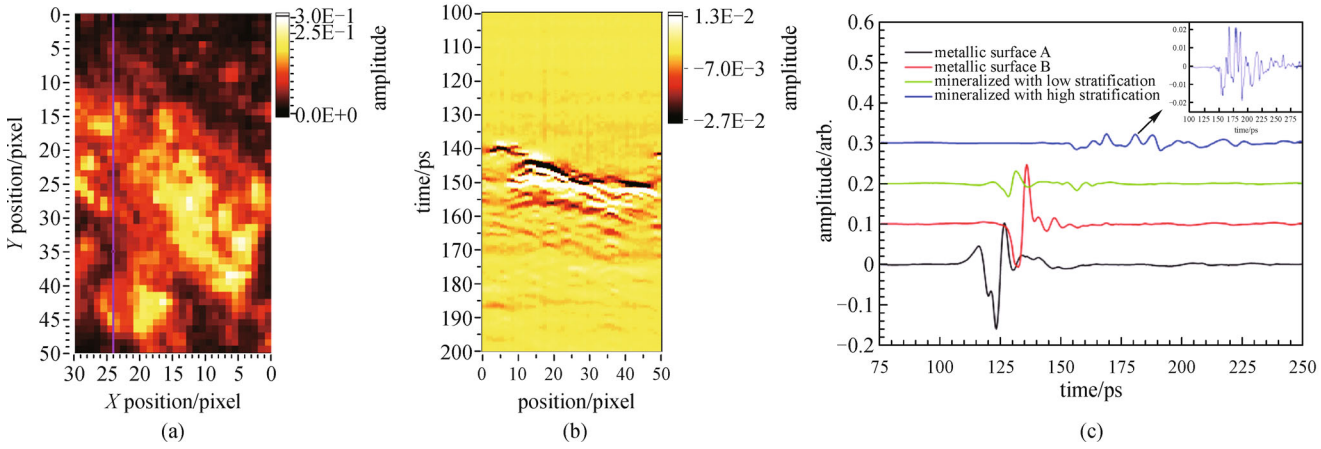

Fig. 10 (a) Peak to peak amplitude terahertz reflection image; (b) cross-sectional b-scan image; and (c) select time-domain signals (offset) [17]

Diyala Valley — were also investigated (Fig. 3). Cup A was covered by dark blue corrosion, presumably azurite crystals with some dark green areas, presumably malachite. The transmission through the base of cup A was at the signal noise floor, therefore the subsurface was still entirely metallic (Fig. 11(a)). Cup B was covered in aqua colored corrosion, an admixture of azurite and malachite, with several regions of dark blue and green. Much of the base of cup B is completely mineralized. The black region of the THz transmission measurement in Fig. 11(b) indicates that approximately 13% of the subsurface area has transmission approaching, but not at, the noise floor, unlike with cup A.

First, we analyzed the minimum peak time-of-flight of both cups. Since no THz signal transmitted through cup A, the image of the minimum peak time was random, as seen in Fig. 12(a). On the other hand, for cup B (Fig. 12(b)), the minimum peak times were locally ordered and fall within a 10 ps time window. This helps to discount the possibility that any dominant pulse in that temporal region is an artificial product of the denoising process, as we would expect it to be random as well. Interestingly, there is not a direct correlation between the peak amplitude and time-of-flight; both regions with the highest and lowest peak amplitudes also have the longest time-of-flights. Additionally, the rim shape of the cup base has no impact on the transmitted peak time, suggesting no change in optical density with deformation for all material components.

Figure 13(a) shows a discrete color map of cup B's transmission factor, defined as

$$\eta = 100\left[\frac{\log\left(E_j/E_{\min}\right)}{\log\left(E_{\max}/E_{\min}\right)}\right], \tag{1}$$

where E_j is the peak to peak amplitude of the time signal for an individual pixel, normalized by $E_{\min}$, the peak to peak amplitude of the smallest pixel signal, and $E_{\max}$ is the peak to peak amplitude of the largest pixel signal

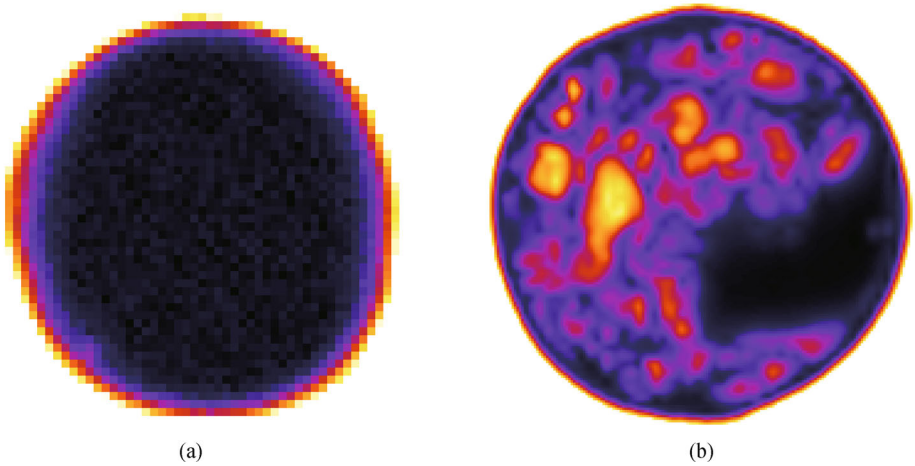

Fig. 11 Transmission images calculated using THz pulse minimum peak amplitude for (a) cup A and (b) cup B {color scale, same: white/yellow = high transmission, black/violet = low transmission}

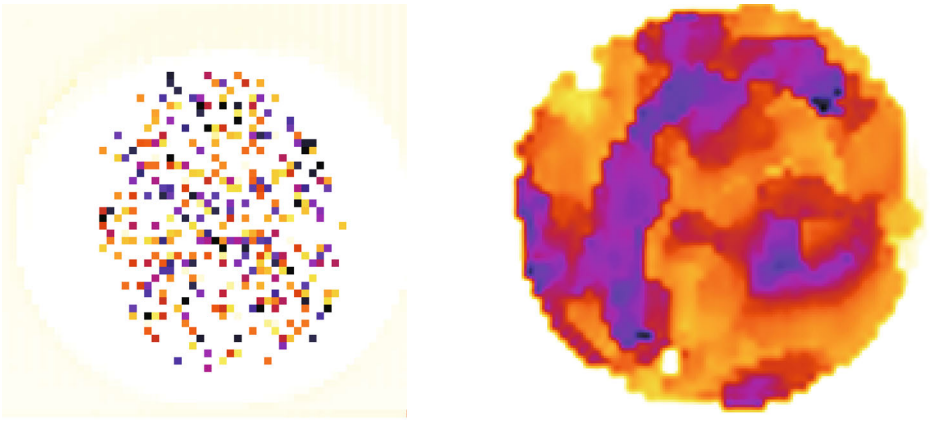

(a) (b)

Fig. 12 Minimum peak time-of-flight for transmission signals through (a) cup A and (b) cup B {color scale, same: white/yellow = shortest time-of-flight [132 ps], black/violet = longest time-of-flight [142 ps]}

(specifically, an air reference). For η greater than 50%, the pattern is consistent with the minimum peak amplitude image in Fig. 11(b). However below 50%, the erstwhile black region now has four levels of intensity with the least transmissive region being reduced to an area approximately 9 mm wide and 36 mm long. The compositional nature of this region is not obvious, although it is probable that this smaller black region describes the location of the only remaining metallic subsurface.

We used Coif4 wavelets with 4 levels to denoise the time-domain waveforms and extract the transmitted signal, shown in Figs. 13(b) and 13(c). Despite an order of magnitude difference in transmission between the wholly-mineralized and partially-mineralized region, there are at least two plausible explanations for the presence of THz signal in the black region of Fig. 13(a). The first possibility is that at least part of that subsurface region is non-transmissive metal, with the full-width, Gaussian-beam diameter exceeding that surface area, resulting in lower frequencies leaking through the surrounding dielectric areas. This is consistent with the "concentric" shape of the blue, red and green regions around the black area, and with the narrow bandwidth, low-central frequency spectra selected as D – H in Fig. 13(c).

On the other hand, it is also plausible that the black region comprises a remnant metallic layer of total thickness less than the skin depth of copper through which the THz pulse is propagating. If the skin depth of copper is given by [24]

$$\sqrt{4300/\nu}, \tag{2}$$

where ν is the THz frequency, then the total thickness of any remnant metal must be less than 75 nm, since there is signal up to 0.6 THz. The likelihood of such a fine layer of copper is worth considering and intriguing, given the totality of the cup's oxidation, and the frequency independent attenuation of metal.

The bases of both cups (Fig. 14) were also measured in reflection. Figure 15(a) shows the image of cup A, calculated using the minimum peak amplitude of the reflected THz pulse. There was significant loss around the edges, due to the increased curvature; however, the reflectivity of the surface is very sensitive to the thickness

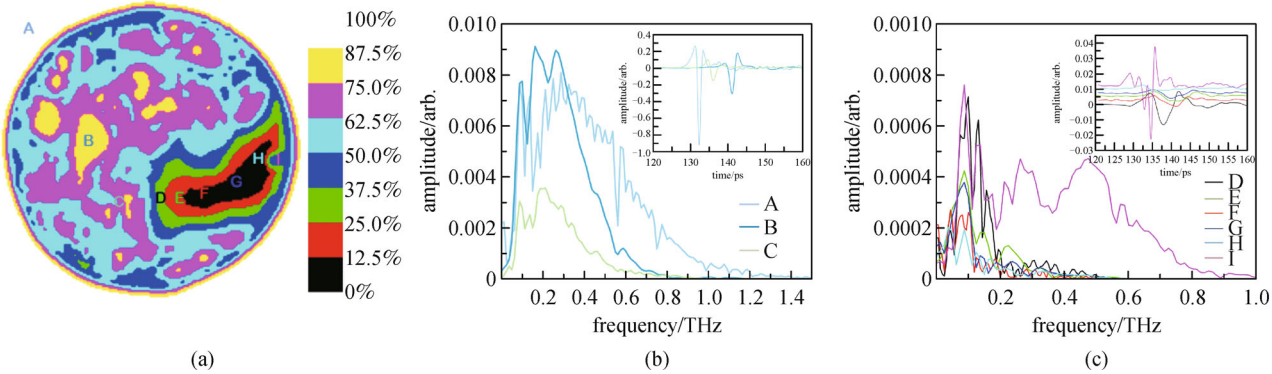

(a) (b) (c)

Fig. 13 (a) Transmission factor, η, map of cup B; (b) and (c) select frequency- and time-domain (inset) waveforms

(a) (b)

Fig. 14 Photographs of the bottom sides of (a) cup A and (b) cup B

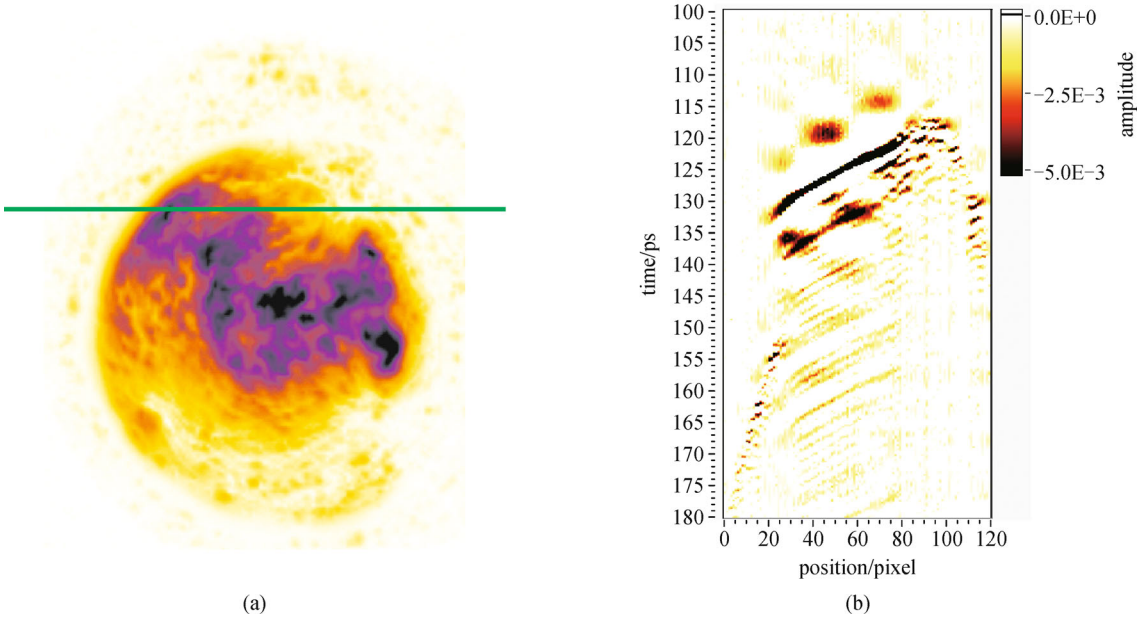

(a) (b)

Fig. 15 (a) Terahertz pulse reflection minimum peak image of cup A {color scale: white/yellow = low reflection, black/violet = high reflection}; and (b) select cross-sectional b-scan, sliced at green line in (a)

and number of corrosive layers. Figure 15(b) shows the b-scan — or cross-sectional signal amplitude image, with vertical axis corresponding to time and the horizontal axis corresponding to the space — of the slice denoted by the green line in Fig. 15(a). This cross-section shows that in the violet areas, there are only two large reflections — one on the mineral surface and one on the metal surface. In the orange area, extra lines appear in the cross-section between the two strongest reflections, suggesting one or two different corrosion layers, whereas, in the yellow area, the reflections are the weakest and the cross-section shows that the yellow and white area is highly stratified.

Figure 16 shows the minimum peak image and a cross-sectional b-scan for cup B. Similarly to cup A, the shape of the base had an impact on the image patterns. A few clusters of higher reflectivity are visible in Fig. 16(a), but none provide insight into the nature of the low transmission area in Fig. 13. The b-scan in Fig. 16(b) is a slice from this area. Interestingly, it shows that between pixels 85 and 35 (left), there are four widely spaced interfaces, separated by 5 – 10 picoseconds; while between pixels 35 and 15 (right), there are thinner, intermediate layers and the reflections lose intensity at a depth equivalent to the second of the left side's layers. This may be the depth of the metallic layer.

Figure 17 shows a reflection image of cup B, calculated

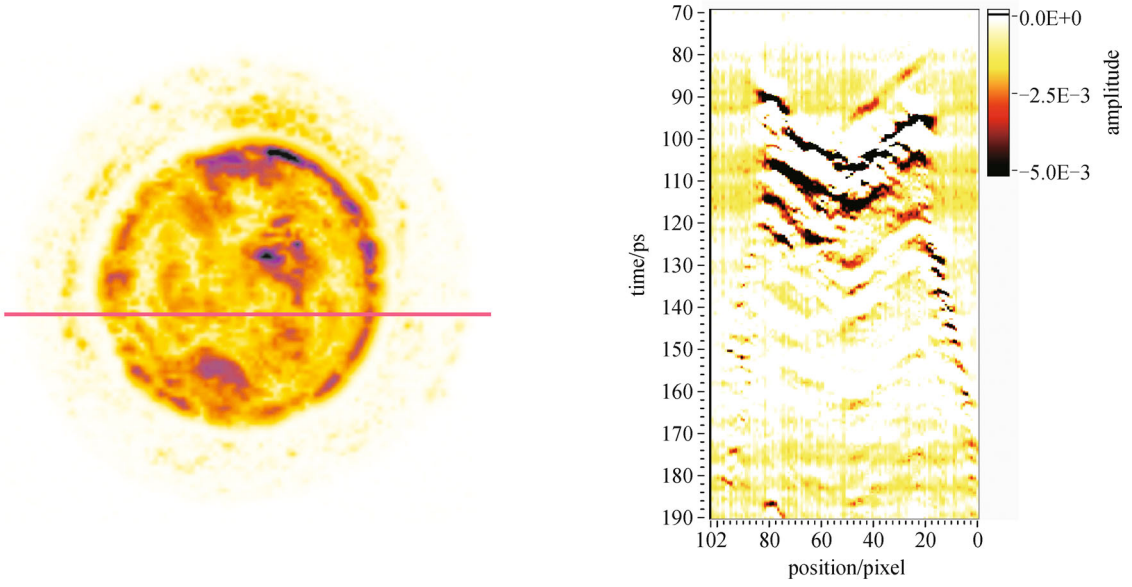

Fig. 16 (a) Terahertz pulse reflection minimum peak image of cup B {color scale: white/yellow = low reflection, black/violet = high reflection}; and (b) select cross-sectional b-scan, sliced at pink line in (a)

by integrating the spectrum of each pixel from 1.0 to 2.0 THz. In this spectral range, there is not much variation in the reflectivity of the mineral clusters. However, what is most noticeable is the resemblance of the violet (i.e., the most reflective) region shape to that of the black area in Fig. 13(a). This reinforces the notion that the material beneath the surface is not predominantly absorbing, but highly reflective and probably metallic in nature. The dimensions are slightly narrower and better defined in the reflection image, which could be attributed to the smaller beam spot size attributable to the shorter focal length lens used.

4 Conclusions

In this paper, we have shown that THz pulsed imaging may be useful to archaeologists and conservation scientists for the non-destructive study of artifacts. Compared to other imaging modalities, portable THz systems can provide more flexibility in the measurement geometry and scale, and convenience by permitting the system to be taken to the object's location. While the spatial resolution is not as detailed as in X-ray imaging, and there is significant signal loss as the object scale increases, we have demonstrated that THz imaging is better able to resolve contrast in the low density components of an ancient Egyptian bird mummy. Additionally, through measurements of ancient Sumerian copper alloy artifacts, we have shown that TPIS can be used for the identification of copper corrosion layers. It can differentiate between metallic and mineralized layers and can qualitatively distinguish different corrosion products.

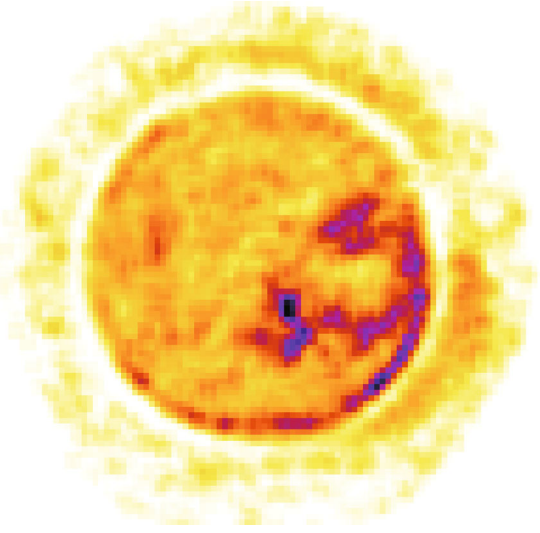

Fig. 17 Frequency-domain power integration between 1.0 and 2.0 THz image of cup B {color scale: white/yellow = low reflection, black/violet = high reflection}

Acknowledgements This work was supported by the European Commission's Seventh Framework Program CHARISMA (Grant No. 228330) and the Marie Curie Intra-European project TISCH (Grant No. 330442). The authors would also like to thank Charles A. Pelizzari—associate professor and director of medical physics in the Department of Radiation and Cellular Oncology at the University of Chicago—and Christian Wietholt—an

application engineer working for visage Imaging, Inc. and developer of the Amira visualization software—for their expertise in X-ray computed tomography and imaging modes.

References

1. Jackson J B, Bowen J W, Walker G C, Labaune J, Mourou G A, Menu M, Fukunaga K. A survey of terahertz applications in cultural heritage conservation science. IEEE Transactions on Terahertz Science and Technology, 2011, 1(1): 220–231
2. Öhrström L, Bitzer A, Walther M, Rühli F J. Technical note: terahertz imaging of ancient mummies and bone. American Journal of Physical Anthropology, 2010, 142(3): 497–500
3. Fukunaga K, Cortes E, Cosentino A, Stünkel I, Leona M, Duling I N III, Mininberg D T. Investigating the use of terahertz pulsed time domain reflection imaging for the study of fabric layers of an Egyptian mummy. Journal of the European Optical Society: Rapid Publications, 2011, 6: 11040
4. Schmuttenmaer C A. Exploring dynamics in the far-infrared with terahertz spectroscopy. Chemical Reviews, 2004, 104(4): 1759–1779
5. Dragoman D, Dragoman M. Terahertz fields and applications. Progress in Quantum Electronics, 2004, 28(1): 1–66
6. Chamberlain J M. Where optics meets electronics: recent progress in decreasing the terahertz gap. Philosophical Transactions Series A, Mathematical, Physical, and Engineering Sciences, 2004, 362 (1815): 199–213
7. Walker G C, Bowen J W, Matthews W, Roychowdhury S, Labaune J, Mourou G, Menu M, Hodder I, Jackson J B. Sub-surface terahertz imaging through uneven surfaces: visualizing Neolithic wall paintings in Çatalhöyük. Optics Express, 2013, 21(7): 8126–8134
8. Walker G C, Berry E, Zinovev N N, Fitzgerald A J, Miles R E, Chamberlain J M, Smith M A. Terahertz imaging and international safety guidelines. Proceedings of the Society for Photo-Instrumentation Engineers, 2002, 4682: 683–690
9. Kristensen T T, Withayachumnankul W, Jepsen P U, Abbott D. Modeling terahertz heating effects on water. Optics Express, 2010, 18(5): 4727–4739
10. Chan W L, Deibel J, Mittleman D M. Imaging with terahertz radiation. Reports on Progress in Physics, 2007, 70(8): 1325–1379
11. Adriaens A. European actions to promote and coordinate the use of analytical techniques for cultural heritage studies. TrAC Trends in Analytical Chemistry, 2004, 23(8): 583–586
12. Tonouchi M. Galore new applications of terahertz science and technology. Terahertz Science and Technology, 2009, 2(3): 90–101
13. Jepsen P U, Cooke D G, Koch M. Terahertz spectroscopy and imaging – modern techniques and applications. Laser & Photonics Reviews, 2011, 5(1): 124–166
14. Pelizzari C A, Haney C R, Bailleul-LeSuer R, Brown J P, Wietholt C. Challenges in CT scanning of avian mummies. In: Bailleul-Lesuer R, ed. Between Heaven and Earth: Birds in Ancient Egypt. Chicago: Oriental Institute of the University of Chicago, 2012, 109–118
15. Jackson J B, Mourou G, Labaune J, Menu M. Terahertz pulse imaging of an Egyptian bird mummy. In: Bailleul-Lesuer R, ed. Between Heaven and Earth: Birds in Ancient Egypt. 1st ed. Chicago: Oriental Institute Museum Publications, 2012, 119–122
16. Luo W, Jin R, Qin Y, Huang F, Wang C. Analysis of the corrosion products of the ancient bronzes excavated from Qiaojiayuan tombs. Applied Physics Research, 2010, 2(2): 156–169
17. Jackson J B, Labaune J, Mourou G A, D'Alessandro L, Whyte A, Menu M. Pulsed terahertz investigation of corroded and mineralized copper alloy historical artifacts. In: Proceedings of 2011 International Conference on Infrared, Millimeter, and Terahertz Waves. Houston, USA: IEEE, 2011, 1–2
18. Anastasi R F, Madaras E I. Terahertz NDE for under paint corrosion detection and evaluation. AIP Conference Proceedings, 2006, 820: 515–522
19. Fuse N, Fukuchi T, Takahashi T, Mizuno M, Fukunaga K. Evaluation of applicability of noncontact analysis methods to detect rust regions in coated steel plates. IEEE Transactions on Terahertz Science and Technology, 2012, 2(2): 242–249
20. Zhao G, Ter Mors M, Wenckebach T, Planken P C M. Terahertz dielectric properties of polystyrene foam. Journal of the Optical Society of America. B, Optical Physics, 2002, 19(6): 1476–1479
21. Banerjee D, von Spiegel W, Thomson M D, Schabel S, Roskos H G. Diagnosing water content in paper by terahertz radiation. Optics Express, 2008, 16(12): 9060–9066
22. Roman C, Ichim O, Sarger L, Vigneras V, Mounaix P. Terahertz dielectric characterisation of polymethacrylimide rigid foam: the perfect sheer plate? Electronics Letters, 2004, 40(19): 1167–1169
23. Fletcher J R, Swift G P, Dai D, Levitt J A, Chamberlain J M. Propagation of terahertz radiation through random structures: An alternative theoretical approach and experimental validation. Journal of Applied Physics, 2007, 101(1): 013102
24. McKnight S W, Stewart K P, Drew H D, Moorjani K. Wavelength-independent anti-interference coating for the far-infrared. Infrared Physics, 1987, 27(5): 327–333

Dr. J. Bianca Jackson is a Marie Curie IntraEuropean Postdoctoral Research Fellow at the University of Reading under the program TISCH: Terahertz Imaging and Spectroscopy for Cultural Heritage. Born and raised in East Orange, New Jersey, she received her bachelor's degree in Applied Physics from Columbia University's Fu Foundation School of Engineering and Applied Science in 2000. She received her M.S. (2005) and Ph.D. (2008) degrees in Applied Physics from the University of Michigan, under the supervision of Dr. John F. Whitaker at the Center for Ultrafast Optical Science (CUOS). There she specialized in nondestructive applications of time domain terahertz imaging and spectroscopy, with particular interest in the measurement and diagnostics of multilayered material systems. In 2008, under the advisement of Drs. Gerard Mourou and Michel Menu, she became a postdoctoral research scientist in Paris, France working through Ecole Polytechnique's Institute de la Lumière Extrême (ILE) and Laboratoire d'Optique Appliquée (LOA), as well as the Laboratoires

de le Centre de la Recherche et de la Restauration des Musées de France (LC2RMF) to construct a terahertz imaging and spectroscopy laboratory specializing in cultural heritage conservation science at the research facility located at the Palais du Louvre. Dr. Jackson was a Chateaubriand Science Fellow (2009 – 2010) and Rackham-NSF Merit Fellow (2001 – 2006). She was also a University of Rochester Postdoctoral Fellow for Diversity and Academic Excellence (2012 – 2013) working at the Institute of Optics at the University of Rochester under Dr. Xi-Cheng Zhang, director of the Institute.

Her terahertz research application interests include fresco wall paintings, wood panel paintings, wooden objet d'art, ceramics and corroded metal artifacts. In her free time, she considers herself a bit of a comedy nerd, and enjoys cooking and reading novels.

Dr. Julien Labaune was born in Clamart, France, in1983. He graduated from the Ecole Normal Superieure de Lyon, and received his M.S. and Ph.D. degrees in Physics from Ecole Polytechnique. He currently works as an engineer at ONERA, the French aerospace research center, in the department of Mesures Physiques/Unité Foudre, Plasmas et Applications.

Rozenn Bailleul-LeSuer is a Ph.D. candidate in Egyptology in the Near Eastern Languages and Civilizations Department of the University of Chicago. She was also guest curator at the Oriental Institute Museum for the special exhibit *Between Heaven and Earth*: *Birds in Ancient Egypt*. After studying Chemical Engineering in Lille, France (Hautes Études Industrielles), and completing a MA in Greek & Latin at the University of Vermont, she is now able to combine her passion for birds and her academic interest in ancient Egypt. She is finishing her dissertation entitled "The Exploitation of Avian Resources in Ancient Egypt: A Socio-Economic Study". Her research incorporates an in-depth study of Egyptian bird mummies, using various imaging techniques, such as CT scanning and THz imaging.

Laura D'Alessandro is head of the conservation laboratory at the Oriental Institute, University of Chicago. She holds a B.A. in Classical Civilizations from the State University of New York at Albany and graduated from the Institute of Archaeology, University of London with a degree in the conservation of archaeological and ethnographic materials. She focuses on the preservation of cultural heritage in the Middle East. Her current research interests includes the aging properties of Egyptian blue and Egyptian green pigments.

Alison Whyte is an objects conservator at the Oriental Institute, where she has specialized in the preservation of archaeological material from the ancient Near East since 2001. She holds a B.A. in Anthropology from the University of British Columbia and a M.A. in Ancient Studies from the University of Toronto. Ms. Whyte is a graduate of the Queen's University Master of Art Conservation Program and is a Professional Associate of the American Institute for Conservation. Her research interests include ancient pigments and glazes and soluble salt efflorescence in archaeological material.

John W. Bowen was born in Malvern, UK, in 1963. He received the B.Sc. degree in Physics from Queen Mary College, University of London, UK, in 1985, and the Ph. D. degree from the University of London in 1993 for his work on techniques for wideband millimetre wave spectrometry.

He took up a lectureship at the University of Reading in 1993 and is now Associate Professor in Cybernetics, in the School of Systems Engineering, Reading, UK. He has authored over 120 academic publications in the field of millimeter wave and terahertz technology. His research interests include the development of terahertz systems and techniques, quasi-optics, terahertz spectroscopy of biological systems and terahertz applications in art and archaeology.

Dr. Bowen is a Chartered Physicist. He is a member of the Institute of Physics, a member of the Optical Society of America, the Society of Photo-optical Instrumentation Engineers and the European Optical Society. He was the sole winner of the 1989 National Physical Laboratory Metrology Award for his invention of a wideband millimeter wave noise source.

Michel Menu was born in France in 1953. He received the Dipl.Ing. degree from l'Université Paris XI—Orsay, in 1976, the Doctorate d'Ingénieur degree in Physics and Optics from l'Université Pierre et Marie Curie—Paris VI in 1978, and the Diplôme d'Habilitation à diriger des rechereches en sciences in 1992.

He has worked at the Research Laboratories of French Museums (now the L-C2RMF) in Paris, France, since 1980, and is currently the chief of research. He has been an author on over 200 scientific publications.

Dr. Menu is a member of the Editorial board of *Applied Physics A* and is the chief editor of *TECHNE*.

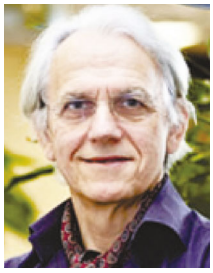

Gerard Mourou was born in La Voulte Ardeche, France, in 1944. He received the B.Sc. degree in Physics from the University of Genoble, France, in 1967, the M.Sc. degree in Physics from the University of Orsay, in 1970, and the Ph.D. degree in Physics from the University of Paris VI, in 1973.

He is currently the Director of the IZEST—the International Center for Zettawatt-Exawatt Science and Technology—a professor of physics at Ecole Polytechnique and professor emeritus at the University of Michigan—where he was the A.D. Moore Distinguished University Professor of electrical engineering and computer science. He was the founding director of the NSF funded Center for Ultrafast Optical Science at the University of Michigan. He is a consultant to several private and governmental organizations, including Lawrence Livermore National Laboratory and Xerox Corporation.

Dr. Mourou has been a pioneer in the field of ultrafast photonics for nearly twenty years. He is recognized worldwide for his work in ultrafast science and technology, having made major contributions covering the field of electronics, optoelectronics, archeology and medicine. He is also the recipient of numerous awards including the Einstein Chair from the Chinese Academy of Science and the Chevalier de la Legion d' Honneur.